PERGAMON

International Journal of Heat and Mass Transfer 45 (2002) 4621–4630

International Journal of HEAT and MASS TRANSFER

www.elsevier.com/locate/ijhmt

# Combined thermocapillary and natural convection in rectangular containers with localized heating

Kyu-Jung Lee [a], Yasuhiro Kamotani [b,*], Shinichi Yoda [c]

[a] Department of Mechanical Engineering, Korea University, Seoul, South Korea

[b] Department of Mechanical and Aerospace Engineering, Case Western Reserve University, 412 Glennan Building, 10900 Euclid Avenue, Cleveland, OH 44016-7222, USA

[c] National Space Development Agency of Japan, Tsukuba, Ibaraki 305-8505, Japan

Received 15 March 2002; received in revised form 16 April 2002

**Abstract**

Combined thermocapillary and natural convection in rectangular containers is investigated experimentally and theoretically. The fluid is heated by a thin wire placed along the free surface. In the parametric range investigated herein, buoyancy alters the thermocapillary flow significantly. The flow field is confined to a relatively small region near the free surface due to thermal stratification. The vertical dimension of the flow cell is determined by a scaling analysis, and the scaling law is shown to agree well with the results from the numerical simulations. The experiment shows that the steady two-dimensional flow field becomes oscillatory and three-dimensional beyond a certain temperature difference. The oscillatory flow field is described based on a flow visualization and temperature measurement. The critical temperature difference for the onset of oscillations is determined under various conditions. It is discussed that the flow becomes oscillatory when the convection in the flow cell becomes sufficiently large. A parameter is derived to represent this convection including the effect of stratification, which is shown to correlate the experimentally determined critical conditions well.



## 1. Introduction

Since the early seventies much attention has been given to oscillatory thermocapillary convection under various conditions. The past experimental work on the subject has recently been reviewed [1]. Many experiments have been performed in the so-called half-zone configuration, mainly with high Prandtl number fluids. Although emphasis is on thermocapillary flow, buoyancy cannot be neglected in some experiments performed in normal gravity. The main objective of the present work is to investigate the interaction between thermocapillary flow and buoyancy.

The present experiment is performed in rectangular containers. Steady flows due to combined thermocapillary and buoyant driving forces in rectangular cavities or slots have been investigated experimentally and theoretically by several investigators (e.g. [2–5]). Pertinent to the present work is the work by Schwabe and Metzger [6], in which the top portion of the fluid layer is subjected to a larger temperature difference than the bulk region. In this situation they showed that the flow is active mostly in the region near the free surface. No oscillations were reported in their work. Oscillatory flows in rectangular cavities have been investigated experimentally [7,8]. It is known from these studies that the steady two-dimensional flow in a cavity changes to steady, three-dimensional flow after the first instability, and then, with a further increase in the imposed temperature difference, it transitions to oscillatory flow. In the present work, the fluid is heated locally by a thin wire placed along the free surface. This heating promotes thermal stratification as in the work by Schwabe and Metzger [6], but without the presence of a large hot wall it is found that the flow becomes oscillatory at a

* Corresponding author. Tel.: +1-216-368-6455; fax: +1-216-368-6445.

*E-mail address:* yxk@po.cwru.edu (Y. Kamotani).

0017-9310/02/$ - see front matter 
PII: S0017-9310(02)00163-1

**Nomenclature**

| | |
|---|---|
| Ar | liquid layer aspect ratio, $H/L$ |
| $D_H$ | diameter of heating wire |
| $Gr$ | Grashof number, $g\beta\Delta TL^3/\nu^2$ |
| $g$ | gravitational acceleration |
| $H$ | liquid layer depth |
| $H^*$ | thermal penetration length scale |
| Hr | heater ratio, $D_H/2L$ |
| $L$ | container half-width |
| $Ma$ | Marangoni number, $\sigma_T\Delta TL/\mu\alpha$ |
| $Ma_{cr}$ | critical Marangoni number |
| $Ma^*$ | modified Marangoni number, $Ma(\sigma_T/\rho g\beta L^2)^{2/3}$ |
| $Ma^*_{cr}$ | critical modified Marangoni number |
| $Nu$ | Nusselt number |
| $Pr$ | Prandtl number, $\nu/\alpha$ |
| $R\sigma$ | Reynolds number, $\sigma_T\Delta TL/\mu\nu$ |
| $T$ | temperature |
| $T_C$ | cold wall temperature |
| $T_H$ | heating wire temperature |
| $U_0$ | maximum velocity in heated region |
| $U_r$ | characteristic velocity of flow |
| $(u, v)$ | velocity components |
| $W$ | container dimension normal to $x$–$y$ plane |
| $(x, y)$ | coordinate system defined in Fig. 1 |
| $\alpha$ | thermal diffusivity |
| $\beta$ | volumetric expansion coefficient |
| $\Delta T$ | imposed temperature difference, $T_H - T_C$ |
| $\Delta T_{cr}$ | critical temperature difference |
| $\zeta$ | vorticity, $\partial v/\partial x - \partial u/\partial y$ |
| $\theta'$ | root-mean-square temperature oscillation level |
| $\mu$ | fluid dynamic viscosity |
| $\nu$ | fluid kinematic viscosity |
| $\rho$ | fluid density |
| $\sigma_T$ | temperature coefficient of surface tension |
| $\psi_{max}$ | maximum stream function, non-dimensionalized by $\sigma_T\Delta TL/\mu$ |

relatively low Reynolds number. Unlike the cavity configuration, the steady two-dimensional flow transitions directly to oscillatory flow. The nature of the oscillatory flow is also different from that found in rectangular cavities.

In addition to the experiment, the basic flow field is investigated numerically, especially concerning the extent of the thermal stratification. Based on the experimental and numerical information, the oscillation mechanism is discussed. It is shown that the stratification plays an important role. A parameter is derived to specify the critical condition for the onset of oscillations.

## 2. Experiments

Fig. 1 shows a schematic view of the test section. Liquid is contained in a rectangular container and is heated along the top free surface by a thin wire at the container center. The sidewalls are cooled to maintain a uniform temperature. Silicone oils with kinematic viscosities of 2 and 5 centistokes (cSt) are used to obtain proper parametric ranges. The test cell consists of two copper end walls, which have cooling channels inside, two clear Plexiglas sides and a Plexiglas bottom. Two different container sizes are used, one with width $L = 1$ cm and length $W$ (the dimension in the spanwise direction of the heater) equal to 6 cm, and the other with $L = 0.75$ cm and $W = 6$ cm. The depth of the test fluid is variable. The temperatures of the copper walls are controlled by constant temperature water circulation.

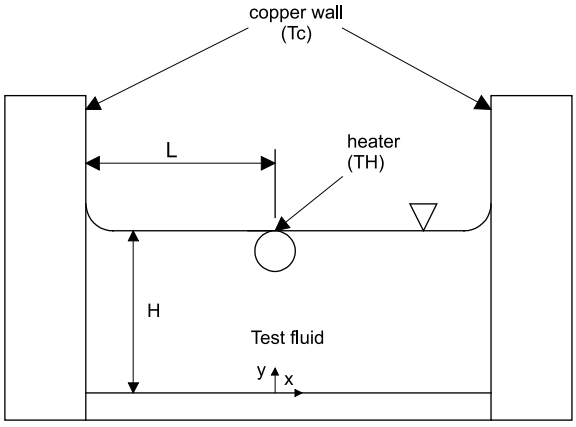


Fig. 1. Schematic of test configuration and coordinate system.

The fluid is heated by a nichrome wire with a 0.65 mm diameter. The wire is submerged in the liquid with its top just touching the free surface from the inside (Fig. 1).

A 0.05 mm diameter copper-constantan thermocouple with its fast response is used for measuring the temperature distribution and the root-mean-square (RMS) temperature oscillation level inside the fluid. The response time is 0.01 s in still water, which is small enough for the present experiment in which typical frequencies are from 0.1 up to 0.7 Hz. The thermocouple is rigid enough so that its position is not influenced by the flow. It is held by a $x$–$y$ traversing holder controlled by two

screws, whose moving scales are measured up to 0.2 mm in the $x$-direction and 0.4 mm in the $y$-direction. In order to measure the temperature of the wire heater, a 0.05 mm diameter thermocouple is attached to the wire at the middle. Two 0.25 mm diameter thermocouples are used for monitoring the temperature of each endwall.

The onset of oscillations is detected by the thermocouple in the fluid and also by flow visualization. The thermocouple probe is placed where the temperature oscillation level has been found to be the largest. Temperature measurements are made with a potentiometer and an Omega-CJ thermocouple cold junction compensator. The thermocouple used for measuring the frequency and RMS oscillation level of the temperature inside the silicone oil is connected to an amplifier with an amplification factor of 1000, and its output is sent to an oscilloscope or a RMS meter. Flow visualization is carried out by adding alumina particles (1–10 μm diameter) to the flow and observing their motions with a microscope and/or a CCD camera.

Since the part of the thermocouple within a few mm from the junction is sensitive to the temperature variation, the thermocouple is placed under the surface along a constant temperature line to reduce the error in temperature measurements. The accuracy of the temperature measurement is estimated to be within 7% of $\Delta T$. The critical temperature difference is reproducible within $\pm 10\%$.

## 3. Ranges of parameters

The important dimensionless parameters for the steady flow are: surface tension Reynolds number ($R\sigma$), Prandtl number ($Pr$), Grashof number ($Gr$), aspect ratio (Ar), relative heater size (Hr). Marangoni number ($Ma = R\sigma Pr$) is also used. The parametric ranges covered in the present experiment are: $Ma < 2 \times 10^4$, $Gr < 7 \times 10^4$, $\mathrm{Ar} = 0.3$–$1.5$, and $\mathrm{Hr} = 0.033$ and 0.043. $Pr$ ranges from 25 to 29 for the 2 cSt fluid and from 47 to 70 for the 5 cSt fluid. The fluid viscosity is evaluated at the average temperature of $T_\mathrm{H}$ and $T_\mathrm{C}$.

The size of the meniscus next to the cold wall is about 2 mm. When the contact line is anchored at the top edge of the cold wall, we can adjust the meniscus size by adjusting the amount of fluid in the container. It is found that the flow and oscillation phenomenon are not appreciably affected by the meniscus size and shape, so we neglect its effect in the present work. The ratio of container length $W$ to liquid depth $H$ varies between 4 and 27 in the experiment, although many data are taken when the ratio is about 6. With the $W/H$ ratio of 4, the side wall effect may not be negligible, but as will be shown later, the oscillation phenomenon is not affected by this ratio even when it is near 4. Therefore, we neglect its effect in the present work.

If we compare the characteristic buoyancy flow velocity, $(g\beta\Delta TL)^{1/2}$ (assuming $\mathrm{Ar} = 1$ for simplicity), with that for thermocapillary flow, $\sigma_\mathrm{T}\Delta T/\mu$, the ratio can be expressed as $Gr^{1/2}/R\sigma$. The parameter is less than 0.1 in the present experiment, so buoyancy flow is relatively weak. However, if we compare the total buoyancy, $\rho g\beta\Delta TL^2$, with the total thermocapillarity, $\sigma_\mathrm{T}\Delta T$, the ratio is $Gr/R\sigma$. The ratio $Gr/R\sigma$ is larger than unity, about 10, in the present experiment. Therefore, thermocapillary flow is the main flow in the present work, but it is significantly modified by buoyancy. This situation is similar to the condition investigated by Schwabe and Metzger [6].

## 4. Numerical analysis

The steady basic flow and temperature fields for the present configuration are numerically analyzed to help us interpret the experimental data. The main objective is to examine how buoyancy affects the flow field when the fluid is heated by a thin wire at the surface. The present numerical scheme is based on the SIMPLER algorithm and has been used in our past thermocapillary flow analyses (e.g. [9,10]). The Cartesian coordinate system is used as drawn in Fig. 1. The flow field is assumed to be two-dimensional with a flat free surface. For simplicity, the cylindrical heater is replaced by a square heater whose hydraulic diameter is equal to the actual heater diameter. The bottom wall is assumed to be thermally insulated. Although the radiative and convective heat loss from the free surface is taken into account (see [10]), in the present experiment, where the cold wall temperature is near the ambient temperature, the loss from the free surface is less than about 5% of the total heat transfer rate through the liquid, so its effect on the steady flow is not important. The fluid viscosity and surface tension vary with temperature. The velocity and stream function are non-dimensionalized by $\sigma_\mathrm{T}\Delta T/\mu$ and $\sigma_\mathrm{T}\Delta TL/\mu$, respectively. The temperature is non-dimensionalized as $(T - T_\mathrm{C})/\Delta T$. The Nusselt number ($Nu$) is defined as the ratio of the total heat transfer rate to the (computed) total conduction heat transfer rate.

A non-uniform grid system is employed with fine meshes around the heater. For a typical condition of $L = H = 1.0$ cm and $\Delta T = 10$ °C with 2 cSt oil ($Ma = 6.0 \times 10^4$, $Gr = 3.0 \times 10^4$, $Pr = 27.1$, and $\mathrm{Ar} = 1$), which is close to the onset of oscillations, the values of maximum dimensionless stream function computed with three different grids, 56 ($x$-direction) × 51 ($y$-direction), $90 \times 80$, and $130 \times 120$ with the smallest mesh sizes next to the heater of $3 \times 10^{-4}$, $1 \times 10^{-4}$, and $5 \times 10^{-5}$, respectively, are $1.12 \times 10^{-3}$, $1.03 \times 10^{-2}$, and $1.02 \times 10^{-2}$. The values of $Nu$ are 8.89, 8.68, and 8.68, respectively. Therefore, the $90 \times 80$ grid system is employed in the present analysis.

## 5. Results and discussions

### 5.1. Steady flow

At first, flow visualization was conducted by adding small particles to the fluid to investigate the steady flow structure. The flow visualization shows two distinct regions, a nearly stagnant region beneath an active flow region. The fluid is heated only near the free surface, so that the hot fluid convected out of the heated region, mainly by thermocapillary flow, tends to stay near the free surface due to buoyancy, which causes a thermal stratification. This thermal stratification confines the active flow field and is an important feature of the present work. As discussed earlier, pure buoyancy-driven flow is much weaker than thermocapillary flow in the present work, since the ratio $Gr^{1/2}/R\sigma$ is less than unity. Moreover, since the fluid is heated by a thin wire at the top, buoyancy acts only in a limited region. For example, according to the present numerical analysis for $\mathrm{Ar} = 1$, the maximum stream function for buoyancy-driven flow alone is generally less than 5% of that for thermocapillary flow alone. Thus, the main effect of buoyancy is to alter the thermocapillary flow by stratification, as discussed earlier.

Typical computed streamline and isotherm patterns are shown in Fig. 2. The flow pattern, showing an active recirculating flow only in the top half of the container, is found to agree well with the flow visualization. There appears a weak counter-clockwise recirculation cell below the main flow cell, the former being driven by the latter against buoyancy. The overall flow field agrees well with the flow pattern picture shown in Schwabe and Metzger [6] when only the top portion of the fluid is heated. An important feature of the thermal field is that the hot fluid is convected along the free surface, turns the cold corner and is pushed downward along the cold wall, which is eventually stopped by buoyancy, thereby limiting the region where the flow is active.

The computed temperature distributions in the fluid are compared with the experimental data in Fig. 3 for $\mathrm{Ar} = 0.8$. They agree well. Similar agreement is also

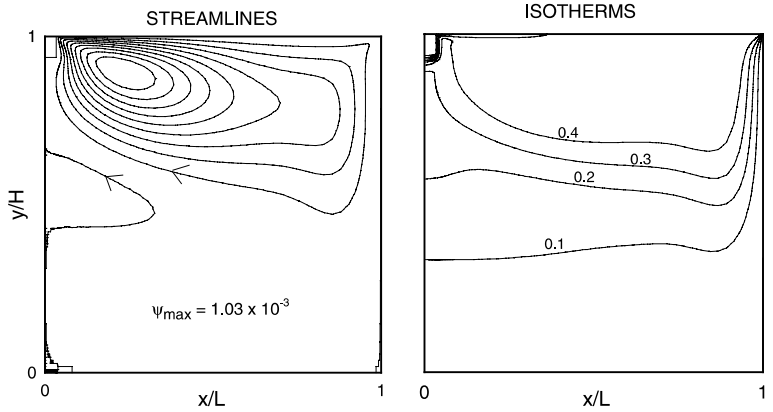


Fig. 2. Computed streamline and isotherm patterns for $Ma = 6.0 \times 10^4$, $Gr = 3.0 \times 10^4$, $Pr = 24.5$, $\mathrm{Ar} = 1$, and $\mathrm{Hr} = 0.035$.

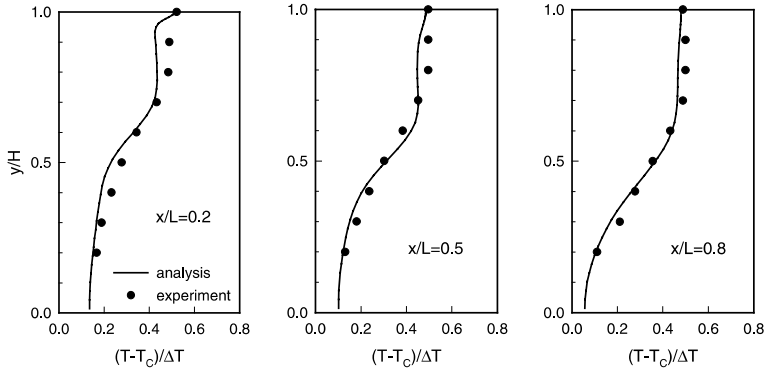


Fig. 3. Comparison between numerical and experimental temperature distributions ($Ma = 6.0 \times 10^4$, $Gr = 3.0 \times 10^4$, $Pr = 27.1$, $\mathrm{Ar} = 0.8$, and $\mathrm{Hr} = 0.035$).

found in other situations, so the present numerical simulations represent the actual tests well. Fig. 3 shows that the fluid temperature is nearly uniform in each of the active and stagnant regions, with large gradients in between.

Since the active flow region does not extend to the bottom when the fluid is deep, container depth $H$ is not important for the flow in this situation. Thus, it is important to know how far the active flow field extends under various conditions in order to understand the basic flow field. Scaling analysis is performed to determine this thermal penetration length ($H^*$). As discussed above, buoyancy opposes the main flow as hot fluid penetrates into the stagnant region along the cold wall. Since buoyancy and thermocapillarity do not act in the same direction, we relate them through the vorticity equation. For two-dimensional steady flow the dimensional vorticity equation is

$$u\frac{\partial\zeta}{\partial x}+v\frac{\partial\zeta}{\partial y}=v\left(\frac{\partial^2\zeta}{\partial x^2}+\frac{\partial^2\zeta}{\partial y^2}\right)+g\beta\frac{\partial T}{\partial x} \tag{1}$$

Thermocapillarity is felt by the flow through the viscous term in the $y$-direction ($v\partial^2\zeta/\partial y^2$). Then, this viscous term should be balanced by the buoyancy term. The viscous term scales as $vU_r/H^{*3}$, where $U_r$ is the characteristic dimensional velocity of the flow in the $x$-direction, and the buoyancy term scales as $g\beta\Delta T/L$. Then, by equating them one obtains $H^*\sim(vLU_r/g\beta\Delta T)^{1/3}$. From our earlier analysis for thermocapillary flow [11], we know that the velocity distribution along the free surface has a peak near the hot wall, and this peak velocity ($U_0$) represents the characteristic velocity of the overall flow because the flow is driven mainly near the hot wall in the case of high $Pr$ fluid. Our analysis also shows that this velocity scales mainly with $\sigma_T\Delta T/\mu$ and only weakly on $Ma$, or the dimensionless velocity scale is nearly constant. Then if we neglect the dependence on $Ma$, we obtain the following scaling law for $H^*$:

$$H^*/L\sim(\sigma_T/\rho g\beta L^2)^{1/3}=(R\sigma/Gr)^{1/3} \tag{2}$$

The peak velocities computed under various conditions are shown in Fig. 4. As will be discussed later, the onset of oscillations occurs in the range of $Ma$ between $5\times10^4$ and $2\times10^5$ in the present experiment. In this range of $Ma$, the dimensionless $U_0$ is nearly constant and depends only very weakly on $Ma$ (roughly $Ma^{-0.07}$), as mentioned above. One important feature of the flow field can be seen by comparing the maximum stream function ($\Psi_{max}$), which represents the overall volume flux in the flow cell, in normal gravity and that in zero gravity. As shown in Fig. 5, since the flow extends to the bottom wall in zero-g, $\Psi_{max}$ is much larger than in one-g. In one-g, buoyancy limits the flow field in such a way that $\Psi_{max}$ is nearly constant in the present experimental range of Ar (Ar $\geqslant$ 0.4). Fig. 5 also shows that when the fluid is very shallow (Ar $<$ 0.4), buoyancy has no appreciable effect on the flow.

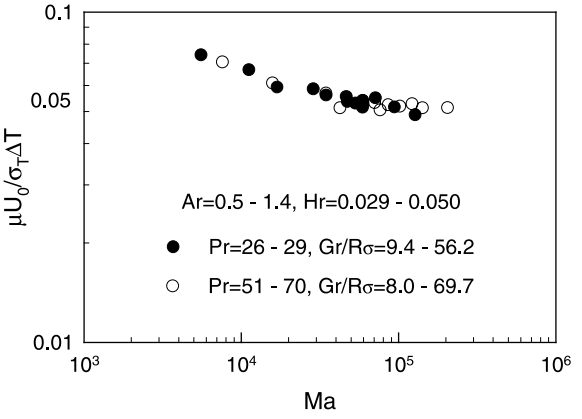


Fig. 4. Maximum free surface velocity near hot wall.

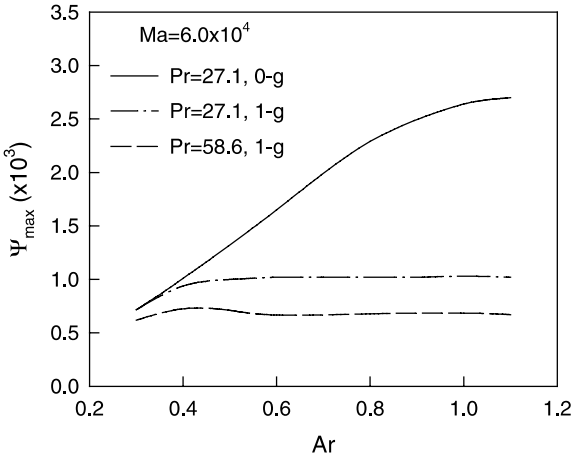


Fig. 5. Maximum stream function versus Ar in one-g and zero-g.

As seen in Fig. 4, $U_0$ is not affected by $Pr$, which means the flow is viscous-dominated. The fact that $\Psi_{max}$ is a function of $Pr$ in Fig. 5 is not due to the inertia forces. The difference is partially due to the difference in $H^*$ between the two fluids for the condition of Fig. 5 and partly due to the difference in viscosity variations. For the conditions of Fig. 5, the overall viscosity variation from the hot to cold walls is about 8% for the 2 cSt fluid, while the variation is 51% for the 5 cSt fluid.

In order to determine $H^*$ from the numerical simulations, we define it as follows. By examining the isotherm and streamline patterns and the temperature distributions in the fluid, such as shown in Figs. 2 and 3, we notice that the isotherms having a dimensionless temperature of between 0.2 and 0.4 are always located in the region of large vertical temperature gradients,

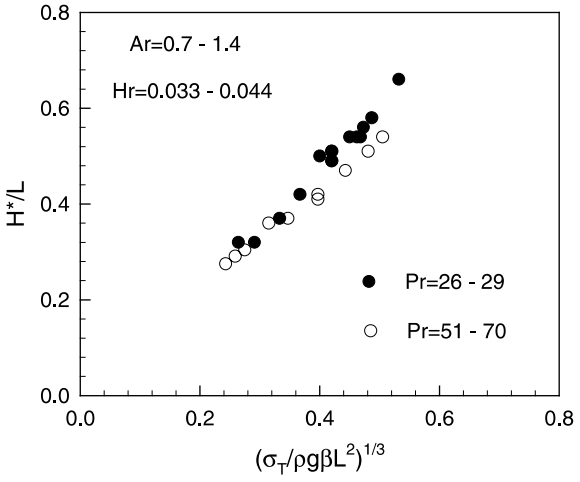


Fig. 6. Thermal penetration length scale.

namely along the interface of active and stagnant regions. For this reason, from the isotherm pattern for a given condition, we define the distance between the free surface and the lowest location of the 0.2 isotherm as the thermal penetration length $H^*$ for this condition in the present work. The values of $H^*$ determined under various conditions are presented in Fig. 6, which shows that the above scaling law for $H^*$ agrees well with the numerical results. $H^*$ is a weak function of $Pr$ due to the difference in the overall viscosity variation, as discussed above. When the parameter $R\sigma/Gr$ becomes very small or very large, buoyancy flow or thermocapillary flow eventually dominates and the flow extends to the bottom, so no $H^*$ exists. Therefore, $H^*$ exists only when the parameter $(R\sigma/Gr)^{1/3}$ is roughly of order unity.

According to Eq. (2), $H^*$ does not depend on $\Delta T$, which we observe experimentally. In the present experiment, the parameter $(\sigma_T/\rho g\beta L^2)^{1/3}$ ranges between 0.42 and 0.51, so $H^*$ is about half of the container depth for $Ar = 1$. As seen in Figs. 4 and 6, within the range of the heater ratio of the present experiment ($Hr = 0.033 - 0.047$), Hr does not affect the scaling laws appreciably. Therefore, we can neglect the heater size effect on these quantities in the present experiment. For later use, we express $H^*$ as

$$H^*/L = C(\sigma_T/\rho g\beta L^2)^{1/3} \tag{3}$$

Based on the numerical results shown in Fig. 6, the values of $C$ are 1.2 and 1.1 for the 2 and 5 cSt fluids, respectively.

When the fluid depth becomes smaller (decreasing Ar), the flow cell eventually reaches the bottom wall. Based on the flow visualization and numerical simulations, a part of the main flow cell touches the bottom wall below Ar of about 0.8 in the present experiment. Since the main cell extends to about the mid-depth for $Ar = 1$, the bottom wall effect becomes very significant below $Ar = 0.5$.

### 5.2. Oscillatory flow

As the temperature difference is increased, the flow field remains two-dimensional (except very near the side walls) according to the flow visualization. Then, at a certain $\Delta T$, the flow transitions to oscillatory flow. The temperature difference at this transition is called the critical temperature difference, $\Delta T_{cr}$. Beyond $\Delta T_{cr}$, temperature oscillations with nearly sinusoidal pattern are observed. The values of $\Delta T_{cr}$ measured under various conditions are plotted in Fig. 7. The figure shows that $\Delta T_{cr}$ is nearly proportional to the fluid viscosity. For a given fluid, $\Delta T_{cr}$ is a function of mainly $H$ and is nearly independent of $L$. Although the data scatters, the general trend of $\Delta T_{cr}$ with increasing $H$ for a given fluid is as follows. When the fluid is shallow (Ar near 0.4), $\Delta T_{cr}$ is not sensitive to $H$. Then with increasing $H$, $\Delta T_{cr}$ decreases but when the fluid becomes deep enough (roughly $Ar > 0.8$), $\Delta T_{cr}$ becomes independent of the depth. Although the ratio of the container length ($W$) to the liquid depth is relatively small near $Ar = 1$, about 6, the fact that $\Delta T_{cr}$ is not affected by the liquid depth near $Ar = 1$ implies that the container length has no appreciable effect on the onset of oscillations.

The oscillatory flow pattern is visually investigated. From the flow visualization it is observed that the steady two-dimensional flow changes to the oscillatory flow that has a three-dimensional structure. Fig. 8 presents sketches of the oscillatory flow pattern from the side and top. When the oscillatory flow occurs, two different flow structures are observed and each of them appears periodically. Based on the side view, one is strong thermo-

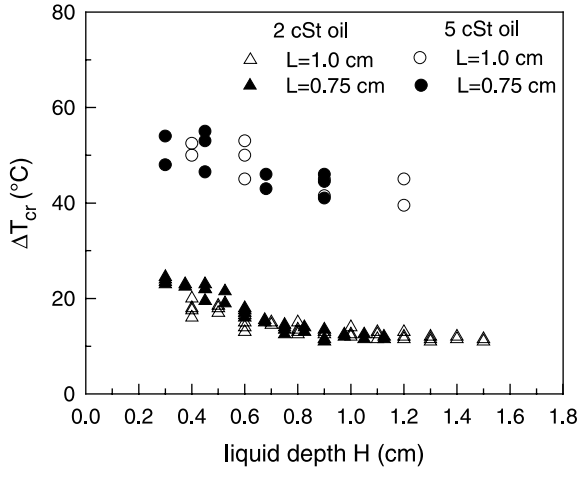


Fig. 7. Critical temperature differences under various conditions.

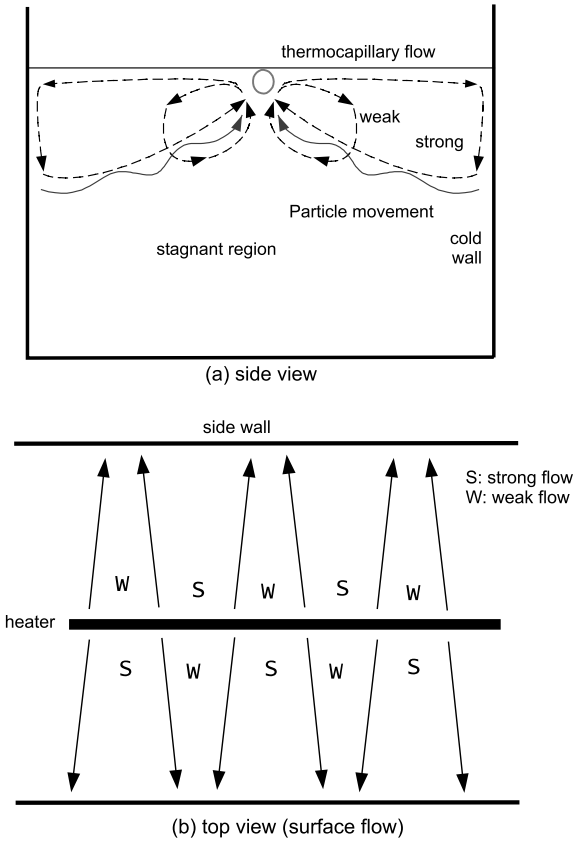


Fig. 8. Sketches of oscillatory flow structure.

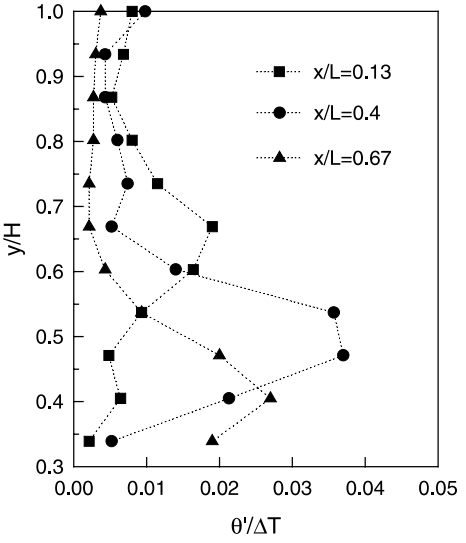


Fig. 9. Temperature oscillation level variations with depth at various $x$ locations ($Ma = 1.2 \times 10^4$, $Gr = 3.8 \times 10^4$, $Pr = 24.5$, $\mathrm{Ar} = 0.83$, $\Delta T/\Delta T_{cr} = 1.8$).

capillary flow that extends all the way to the cold wall, and the other is weak thermocapillary flow that recirculates only near the heater. These two strong and weak periods are similar to those observed in the half-zone configuration [11].

From the top view, these strong and weak structures are arranged periodically in the spanwise direction at any given time. Also, at a given spanwise location the flow structure variation is exactly out of phase across the heater. During the weak period, the flow rate decreases as the fluid moves towards the cold wall, so the flow passage narrows when it is viewed from the top. The opposite happens during the strong period. Also in Fig. 8, the strong and weak patterns appear alternately at the same location, which suggests that no thermal wave is propagating in the spanwise direction. The wavelength of the spanwise pattern is about 1.5 cm in the present experiment. Thus, the container length is four times of this wavelength, which explains why the container length has no appreciable effect on the onset of oscillations in the present experiment.

One interesting feature of the oscillatory flow is that during the strong period, we observe strong downward motion along the cold wall (see Fig. 8), which pushes the interface between the flow cell and the stagnant region downward near the cold wall. The interface moves up during the weak period. This up-and-down motion of the interface does not decay immediately, instead this motion continues, with diminishing amplitude, as the fluid moves from the cold wall region toward the heater region. As a result, the interface becomes wavy during oscillations. Since the vertical temperature gradients are relatively large across the interface, this up-and-down motion causes large temperature oscillations near the interface. The RMS temperature oscillation levels measured at various locations are shown in Fig. 9. As seen in the figure, at a given $x$-location, the oscillation level is highest well inside the fluid, and the maximum temperature oscillation point goes deeper into the fluid with increasing $x$, following the location of the interface. Note that if the inertia forces are strong in the main cell, this interface phenomenon may lead to a Kelvin–Helmholtz type instability.

Fig. 10 shows how the dimensionless RMS temperature oscillation level varies with increasing temperature difference beyond the critical point for various aspect ratios. The oscillation level shown in the figure is the maximum oscillation level at $x/L = 0.4$. When Ar is near unity, the oscillation level increases sharply with increasing $\Delta T$, but when Ar is near 0.5, the increase is more gradual. Therefore, the bottom wall not only delays the onset of oscillations but it also limits the oscillation activities. It is also found that the bottom wall decreases the oscillation frequency (about 0.15 Hz for $\mathrm{Ar} = 0.4$ compared to 0.38 Hz for $\mathrm{Ar} = 1$ with 2 cSt fluid) and distorts the oscillation pattern.

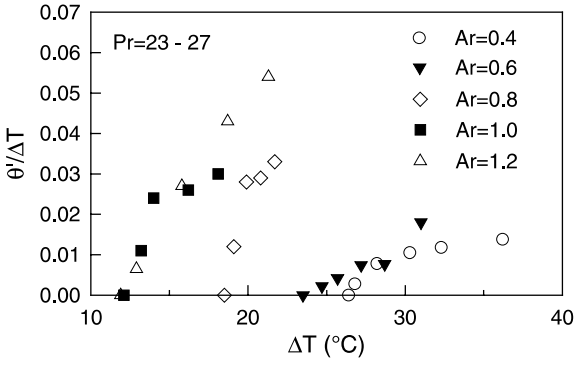


Fig. 10. Temperature oscillation levels with increasing $\Delta T$ for various Ar.

Based on all of this information, we can discuss the oscillation mechanism. When Ar is near 0.4, buoyancy has no appreciable effect on the flow, as discussed earlier. Therefore, the oscillation phenomenon near this Ar is associated mainly with thermocapillary flow. With increasing Ar, the oscillatory flow is modified by buoyancy. Note that although the viscous retardation effect from the bottom wall decreases as Ar increases, this effect is not directly affecting the oscillation phenomenon since the overall flow velocity does not change with Ar (see Figs. 4 and 5). Instead, the bottom wall effect is felt through the aforementioned interaction between the downward flow and buoyancy near the cold wall. This interaction, which plays an important role in the oscillation mechanism, is made easier as the fluid becomes deeper, which explains why $\Delta T_{cr}$ decreases with increasing $H$ until the main flow cell is no longer affected by the bottom wall.

Since the oscillatory flow in the present work is basically caused by thermocapillarity and its structure is similar to that found in the half-zone configuration, we can utilize the information for that configuration to construct a physical model with buoyancy. The basic oscillation process can be described as follows. One oscillation cycle consists of a strong period and a weak period. During the strong period, the flow cell extends to the cold wall so that the heat transfer at the cold wall is increased, which produces colder return flow. When this colder fluid arrives at the heater region, the free surface temperature begins to decrease in this region, which ends the strong period. In the weak period, the heat transfer at the cold wall is small, so the return flow to the heated region is relatively warm, which subsequently heats the free surface and ends the weak period. Now, this basic oscillation process is aided by buoyancy as follows. In the strong period, as the warm fluid is transported to the cold wall region and then turns downward, buoyancy acts to retard the flow near the cold wall. Consequently, the strong flow cell begins to shrink and the slow period starts (see Fig. 8). In the weak period, the fluid that comes near the cold wall is relatively cold, so the flow in this region is eventually revived by buoyancy and the flow cell becomes large again. Therefore, the activity near the cold wall associated with buoyancy is augmenting the oscillation process.

Since the convection across the container determines the oscillation period according to the above oscillation process, the frequency of oscillations should scale as $U_r/L$. As discussed earlier, $U_r$ scales as $\sigma_T \Delta T/\mu$. If we consider the average velocity around $x/L = 0.5$ as the mean convection velocity in the container, the numerical analysis shows that the average velocity is about $0.01\sigma_T \Delta T/\mu$. Then, the frequency scales as $0.01\sigma_T \Delta T/\mu L$ (since this scaling law is for steady flow, we can use this expression only very near the onset of oscillations). For a typical condition of $L = H = 1.0$ cm with 2 cSt fluid, the measured oscillation frequency is 0.38 Hz near $\Delta T_{cr} = 10.8$ °C. According to the scaling law, the estimated frequency is 0.44 Hz, which reasonably agrees with the measured value.

The flow becomes oscillatory when the convection becomes important, so we correlate the critical conditions by the appropriate convection parameter. When the fluid layer is deep, length scale $H^*$ limits the lateral extent of the flow and there exist relatively large vertical temperature gradients along the interface (Fig. 3). Then, the appropriate convection parameter is the ratio of the convection in the $x$-direction, represented by $U_r \Delta T/L$, and the conduction in the $y$-direction, represented by, $\alpha \Delta T/H^{*2}$. The ratio can then be expressed as $Ma^* = Ma(H^*/L)^2$, called the modified Marangoni number herein. $H^*$ represents the effect of buoyancy. On the other hand, when Ar is small (near 0.4), buoyancy is small, and no large vertical temperature gradients exist in the bulk flow. In this situation, the appropriate convection parameter is just $Ma$. Therefore, we correlate the critical conditions for small and large Ar differently.

The values of $\Delta T_{cr}$ are non-dimensionalized as $Ma^*_{cr}$ in Fig. 11 for Ar $\geqslant 0.8$ and as $Ma_{cr}$ for small Ar in Fig. 12. For Fig. 11, the expression for $H^*$ given by Eq. (3) is used. Although the data tends to scatter, the critical conditions seem to be correlated by the convection parameters reasonable well, which supports the above discussions on the basic flow structure and the oscillation mechanism.

It is interesting to compare the oscillatory flow investigated herein with that observed in a two-dimensional cavity with heated and cooled end walls. In the cavity configuration, the heater size, relative to the cold wall size, is much larger than that in the present work. As a result, buoyancy-driven flow is stronger relative to thermocapillary flow for a given $\Delta T$. Thus, under similar conditions as in the present experiment, the overall flow

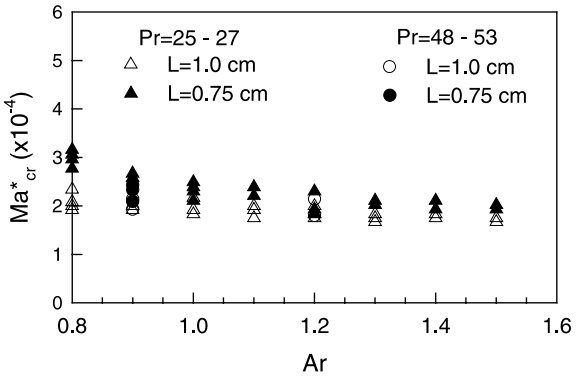


Fig. 11. Critical modified Marangoni number versus Ar for large Ar.

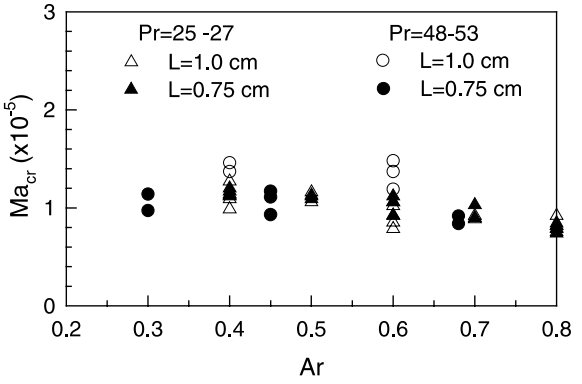


Fig. 12. Critical Marangoni number versus Ar for small Ar.

is active over most of the cavity, so no distinct two-layer structure appears. However, at a larger $\Delta T$ (smaller $Gr^{1/2}/R\sigma$) the flow cell driven mainly by thermocapillarity appears distinctly near the top, as in the present work [6]. In the cavity configuration, the steady two-dimensional flow changes, with increasing $\Delta T$, to three-dimensional steady flow. This transition occurs around $R\sigma$ of $10^4$ for $Pr = 10$ and for Ar of about unity [3]. This flow consists of the main flow from the hot to cold walls and stationary longitudinal rolls. With a further increase in $\Delta T$, this three-dimensional flow becomes oscillatory around $R\sigma$ of $2 \times 10^4$ for Ar near unity when the cavity is large in length [8]. In comparison, in the present configuration, the flow becomes unstable at $R\sigma$ of around $2 \times 10^3$ for Ar near unity. Apparently, the fact that there is no large hot wall in the present configuration makes the flow more susceptible to instability. Since $R\sigma$ is large for the oscillatory flow in cavity, the oscillation mechanism is strongly affected by inertia forces. Sakurai et al. [8] mentions that the oscillation occurs as the rolls go into a wave-like motion. Based on the experiment with shallow enclosures ($Ar \leqslant 0.5$) where the cavity length is equal to the width, Braunsfurth and Homsy [7] describes the oscillation process in which a small eddy close to the hot wall oscillates in both size and strength. In contrast, the present oscillation phenomenon is similar to that in the half-zone configuration, in which inertia forces do not play an important role [11].

## 6. Conclusions

An experiment has been conducted to study combined thermocapillary and natural convection in rectangular containers with high Prandtl number fluids. The fluid is heated by a thin wire. The work is supplemented by a numerical analysis. The following conclusions can be drawn from the work:

(1) In the present experiment, buoyancy acts in such a way that the main recirculating flow cell due to thermocapillarity is pushed upward, and it does not interact with the bottom wall when the aspect ratio is larger than about 0.8. The size of this flow cell due to thermal stratification is determined by scaling analysis. The scaling law agrees well with the numerical result.
(2) The flow remains two-dimensional until it becomes oscillatory at a certain $\Delta T$. The oscillatory flow has a three-dimensional structure with periodic spanwise variation. The flow undergoes strong and weak periods in one cycle of oscillation. The oscillation level is highest along the interface between the main flow cell and the stagnant region below it.
(3) The oscillations are caused by strong convection within the flow cell. The modified Marangoni number ($Ma^*$) is derived for deep fluid, representing the convection and including the effect of the thermal stratification. $Ma^*_{cr}$ correlates the experimental critical conditions well.

## Acknowledgements

This work was partially supported by the National Space Development Agency of Japan. Their support is acknowledged.

## References

[1] M.F. Schatz, G.P. Neitzel, Experiments on thermocapillary instabilities, Ann. Rev. Fluid Mech. 33 (2001) 93–127.
[2] D. Villers, J.K. Platten, Coupled buoyancy and Marangoni convection in acetone: Experiments and comparison with numerical simulations, J. Fluid Mech. 234 (1992) 487–510.

[3] F. Daviaud, J.M. Vince, Traveling waves in a fluid layer subjected to a horizontal temperature gradient, Phys. Rev. E 48 (6) (1993) 4432–4436.
[4] M. Mundrane, A. Zebib, Two- and three-dimensional buoyant thermocapillary convection, Phys. Fluids A 5 (4) (1993) 810–818.
[5] P. Gillon, G.M. Homsy, Combined thermocapillary-buoyancy convection in a cavity: An experimental study, Phys. Fluids 8 (11) (1996) 2953–2963.
[6] D. Schwabe, J. Metzger, Coupling and separation of buoyant and thermocapillary convection, J. Cryst. Growth 97 (1989) 23–33.
[7] M.G. Braunsfurth, G.M. Homsy, Combined thermocapillary-buoyancy convection in a cavity. Part II. An experimental study, Phys. Fluids 9 (5) (1997) 1277–1286.
[8] M. Sakurai, J. Leypoldt, H.C. Kuhlmann, H.J. Rath, Instability of thermocapillary convection in a rectangular cavity under 1g and micro-g conditions, Paper IF-1148, 2nd Pan Pacific Basin Workshop on Microgravity Sciences, Pasadena, CA, May 2001.
[9] Y. Kamotani, S. Ostrach, A. Pline, Analysis of velocity data taken in surface tension driven convection experiment in microgravity, Phys. Fluids 6 (1994) 3601–3609.
[10] Y. Kamotani, S. Ostrach, A. Pline, A thermocapillary convection experiment in microgravity, J. Heat Transfer 117 (1995) 611–618.
[11] Y. Kamotani, S. Ostrach, Theoretical analysis of thermocapillary flow in cylindrical columns of high Prandtl number fluids, J. Heat Transfer 120 (1998) 758–764.